Synthesis, Characterization and Photocatalytic Activity ofAg_2O/Zr-MOF, a Composite of Ag_2O Nanoparticles and Zr-MOF

Md. Ariful Islam[1], Md. Azharul Arafath[1]*, Reazul Hasan Riyan[1], Muhaimin Helal Efat[1] and Md. Sohrab Hossain[2]

[1]Department of Chemistry, School of Physical Sciences, Shahjalal University of Science and Technology, Sylhet 3114, Bangladesh

[2]HICoE-Centre for Biofuel and Biochemical Research, Department of Applied Science, Faculty of Science, and Information Technology, Universiti Teknologi PETRONAS, Seri Iskandar 32610, Perak Darul Ridzuan, Malaysia

*Corresponding author (e-mail: arafath-che@sust.edu)

Ag_2O nanoparticles and an Ag_2O/Zr-CP composite were synthesized by co-precipitation and sonication methods, respectively. The synthesized Ag_2O/Zr-CP composite was characterized by FTIR, UV-Visible spectroscopy, EDS and SEM. FTIR and UV-Visible spectroscopy confirmed the formation of Ag_2O nanoparticles and the Ag_2O/Zr-CP composite. Scanning Electron Microscopy (SEM) confirmed the nanostructures of the synthesized products. Under solar irradiation, the Ag_2O NPs and Ag_2O/Zr-CP composite exhibited photocatalytic activity toward methylene blue (MB) dye at pH 9.2. The degradation efficiencies of the synthesized Ag_2O NPs and Ag_2O/Zr-CP composite were 82.23 % and 83.36 %, respectively. In contrast, TiO_2 exhibited an efficiency of 80.49 %. A kinetic study found that the Ag_2O NPs and the Ag_2O/Zr-CP composite had rate constants of 1.63×10^{-2} min^{-1} and 3.36×10^{-2} min^{-1}, respectively. The pseudo-first-order reaction was followed by photodegradation of the dye, as indicated by the regression values (R^2) of 0.9774 for the Ag_2O NPs and 0.9937 for Ag_2O/Zr-CP. The band gap values for the Ag_2O NPs and Ag_2O/Zr-CP were also determined at 1.62 eV and 1.8 eV, respectively. To increase photocatalytic activity, an optimal band gap is required. The band gap decreased to the ideal value for radical generation when the Ag_2O NPs were added to Zr-CP. Thus, the synthesized Ag_2O/Zr-CP composite may be applied to several industrial processes while advancing environmentally friendly and sustainable technology.

Keywords: MOF; nanoparticle; composite; dye degradation; SEM, methylene blue

Received: May 2025; Accepted: July 2025

Metal-Organic Frameworks (MOFs) are a novel type of material composed of interconnected metal ions and organic molecules. They have a high surface area, and an extensively porous, three-dimensional structure at the nanoscale [1]. Due to their ability to combine different functionalities, MOFs are well-suited for constructing materials with diverse molecular building blocks arranged in a regular, periodic structure [2]. It is feasible to design and produce MOFs that have the optimal pore size, shape, and capacity to store a specific compound [3]. MOFs have captured considerable attention in recent times due to their promising applications across a range of sectors such as gas storage [4], separation [5], heterogeneous catalysis [6-8], ion exchange [9], molecular magnetism [10], biomedicine [11], sensing [12], drug delivery [13], supercapacitors [14], environmental remediation, optoelectronics, and luminescent devices [15].

Coordination polymers (CPs), a subclass of MOFs consisting of metal ions and multidentate ligands, are known for their structural flexibility and chemical stability [16]. These properties make CPs highly suitable for environmental and energy-related applications [17]. CPs are highly effective photocatalysts for removing organic impurities [18]. Owing to their tuneable electronic structures and visible-light absorption, CPs have emerged as efficient photocatalysts for degrading organic pollutants, reducing CO_2, and enabling environmental remediation [19, 20]. The facile design of CPs allows researchers to tailor their functionality by modifying ligands or metal centres, which broadens their application scope in materials science and nanotechnology [21]. MOFs permit multiple bonding interactions between metal ions and light-sensitive organic molecules [22]. MOFs show excellent durability, sustaining their stability through five catalytic cycles. The chemistry of dye degradation involves hydroxyl radicals and holes [23]. MOFs

have excellent potential to form composites with active compounds as they have high porosity and a large surface area. This combination introduces a synergistic effect, tuning the band gap between the valence band and conduction band to the optimum level for more sustainability of the (e/h) pair than immediate recombination; this significantly enhances photocatalytic performance [24]. The ability to construct such hybrid systems by integrating MOFs or CPs with other functional materials, such as nanoparticles, represents a novel strategy for developing high-performance photocatalysts for environmental and energy applications.

Nanotechnology focuses on the development and manipulation of particles in the nanometre range (1-100 nm) using various synthesis methods and modifying their structure and size [25]. Due to their notable features that are beneficial for catalysis, researchers are currently focusing on the synthesis of metal nanoparticles, nanostructures, and nanomaterials [26], as well as composites such as polymer preparations [27]. Nanoparticles (NPs) are a key asset for catalytic applications and are utilized in both industrial and academic research. Metallic nanoparticles (NPs) are applied across multiple domains, including energy, chemistry, biology, and environmental science [28].

Silver-based nanocomposites exhibit an extensive variety of behaviours compared to their parent nanoparticles. Zhang et al. [29] synthesized Ag_2O/g-C_3N_4/Fe_3O_4 nanocomposites by co-precipitation and calcination methods, and these were used in the photodegradation of Rhodamine B (RhB) dye. Ullah et al. [30] synthesized a silver-morphine-functionalized polypropylene adsorbent, which was effectively used for photocatalytic degradation of methyl orange in wastewater. A basic yellow dye, Auramine O (AO), was removed from an aqueous solution using a synthesized Ag_2O nanocomposite [31]. Therefore, combining Ag_2O nanoparticles with zirconium-based coordination polymers (Zr-CPs) results in a composite that improves photocatalytic activity in a synergistic manner.

Despite significant advancements in water treatment technologies, the persistence of synthetic dyes and organic pollutants in wastewater remains a major environmental concern due to their toxicity, stability, and resistance to biodegradation. Conventional methods often fall short in achieving complete and cost-effective degradation of these contaminants. Recent studies suggest that nanostructured materials-particularly metal-organic frameworks (MOFs), coordination polymers (CPs), and metallic nanoparticles like Ag_2O—offer promising photocatalytic capabilities for environmental remediation. However, the synergistic combination of Ag_2O nanoparticles with zirconium-based coordination polymers (Zr-CPs) remains under explored. This study aims to investigate the photocatalytic efficiency of Ag_2O, Zr-CPs, and their composites in the degradation of organic pollutants. The goal is to demonstrate how these materials can be effectively utilized to address wastewater contamination, paving the way for potential industrial applications and sustainable environmental practices.

EXPERIMENTAL

Chemicals & Materials

High-purity $AgNO_3$ (99%) and NaOH (purity ≥ 97 %) were procured from Sigma Aldrich. The model pollutant, methylene blue (MB) (82 %) was purchased from PT. Smart Lab Indonesia. Zr-CP was used as a precursor for composite synthesis. All the chemicals were used as supplied, with no additional purification. Deionized (DI) water was utilized in the stock solutions.

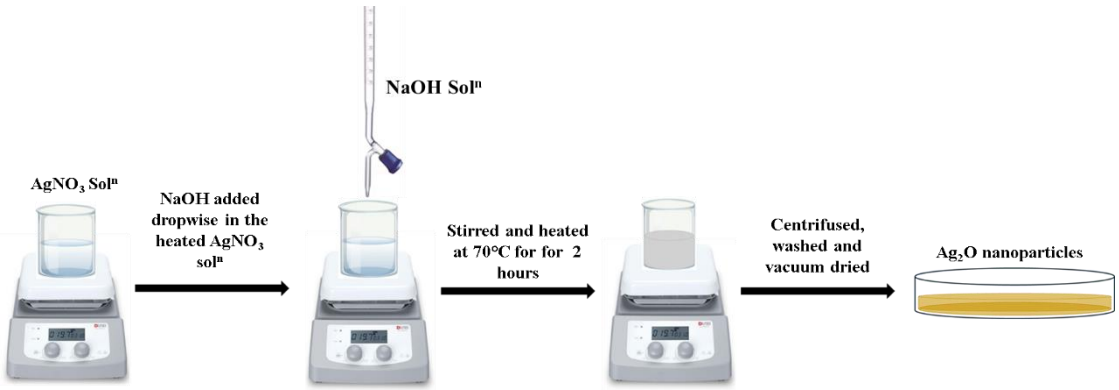

Figure 1. Schematic representation of silver oxide nanoparticles synthesis.

Sample Preparation

Synthesis of Ag_2O NPs

Silver oxide nanoparticles were synthesized by the co-precipitation method. First, 100 mL of 0.015 M silver nitrate ($AgNO_3$) and 20 mL of 0.095 M sodium hydroxide (NaOH) solution were prepared separately in deionized (DI) water. The silver nitrate solution was heated to 70 °C. NaOH solution was added dropwise to the heated $AgNO_3$ solution with continuous stirring. The resultant mixture was stirred and heated to 70 °C for 2 hours. Under these conditions, a greyish colloidal suspension was observed. The colloidal suspension was centrifuged and washed with DI water. The brownish grey product (Ag_2O) was collected. Theproduct's particle structure was preserved by vacuum drying, and it was subsequently kept in a desiccator to prevent moisture absorption.

Synthesis of Ag_2O/Zr-CP Composite

In a 250 ml beaker, 50 mL of a 25 % Ag_2O colloidal suspension was prepared. This was subsequently mixed with 50 mL of a 75 % Zr-CP colloidal suspension by maintaining a 1:3 ratio of Ag_2O nanoparticles and Zr-CP. The resulting suspension was sonicated for 30 minutes to enhance mixing. The product was separated using centrifugation and washed with DI water several times to obtain a greyish Ag_2O/Zr-CP composite. This was dried in a vacuum oven and then stored in a desiccator, as previously described.

Photodegradation of Methylene Blue (MB)

The photodegradation of methylene blue by Ag_2O and the Ag_2O/Zr-CP composite demonstrated their photocatalytic performance. 200 mL of a 5ppm methylene blue solution was prepared using deionized (DI) water. A buffer tablet was used to maintain the pH at 9.2. 10 mg each of Ag_2O and the Ag_2O/Zr-CP composite catalyst were added separately to 100 mL solutions of methylene blue and stirred to ensure uniform dispersion. The solutions were kept in the dark for half an hour to ensure dye removal by adsorption. Then the absorbance of the samples was measured by UV-Vis spectroscopy. The dye solution with the photocatalyst was exposed to sunlight with continuous stirring, and a sample was taken every 20 minutes to measure absorbance. The following formula was used to determine the percentage of dye degradation [32].

$$\textbf{\textit{Degradation efficiency}}\ (\%) = \frac{(C_0 - C_t)}{C_0} \times 100$$

Where C_0 = initial concentration of MB

And C_t = concentration at time t.

Characterization Methods

Fourier-transform infrared (FT-IR) spectra were recorded using an IRTracer-100 (Shimadzu Corporation, Japan) instrument equipped with an ATR (Attenuated Total Reflectance) accessory, over a range of 4,000 to 400 cm^{-1}. A UV-Vis spectrophotometer (Shimadzu UV-1800 Series) was used to record UV-Vis spectra in DI water within the wavelength range of 200 to 800 nm. Scanning Electron Microscopy (SEM) was used to evaluate morphology and microstructure using the EVO18 instrument (Carl Zeiss AG, UK). Energy-dispersive X-ray spectroscopy (EDS) was utilized for elemental analysis and characterization of composition by identifying the distinctive X-rays emitted from the sample during its interaction with a high-energy electron beam.

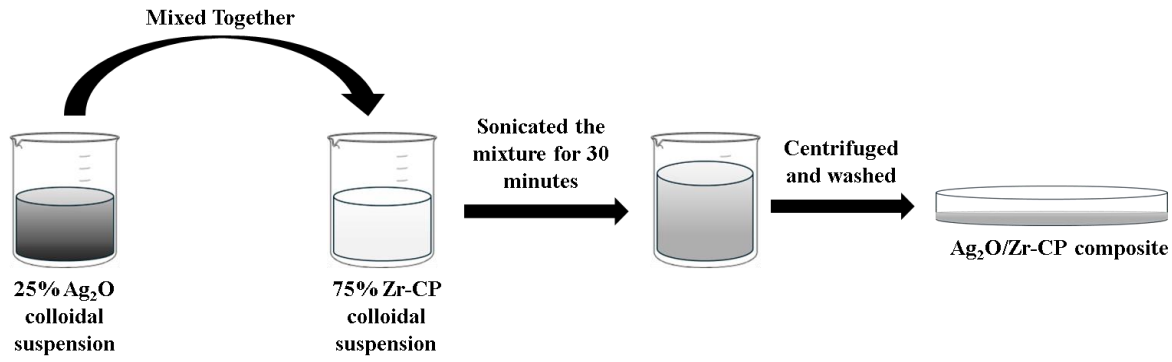

Figure 2. Schematic representation of Ag_2O/Zr-CP composite synthesis.

RESULTS & DISCUSSION

The synthesized Ag_2O and Ag_2O/Zr-CP composite were characterized by several spectroscopic techniques, including UV-Vis spectroscopy, FTIR spectroscopy and Energy Dispersive X-ray Spectroscopy (EDS). Additionally, an advanced imaging technique, Scanning Electron Microscopy (SEM), was also utilized.

FTIR

FTIR spectroscopy was employed to analyse the chemical structure and confirm the formation of the synthesized Zr-CP, Ag_2O nanoparticles (NPs) and Ag_2O/Zr-CP composite. The FTIR spectra of the synthesized products were recorded in the range of 4000–400 cm^{-1}, that showed characteristic peaks corresponding to the functional groups of the individual components, as well as the composite as a whole.

In the FTIR spectrum of the Ag_2O nanoparticles, the peak at 883.39 cm^{-1} corresponds to Ag–O stretching, while the peak at 1381.03 cm^{-1} is attributed to nitrate ions (NO_3^-), likely due to residual silver nitrate that was used during synthesis [33]. Stretching vibrations observed in the IR spectrum of Zr-CP at 1689.64 cm^{-1} and 1404.17 cm^{-1} are attributed to C=O and C=N stretching, respectively.

In the Ag_2O/Zr-CP composite, peaks appeared at 1631.77 cm^{-1} and 789.34 cm^{-1}, corresponding to C=O stretching and Ag–O vibrations. The Ag–O peak shifted from 883.39 cm^{-1} to 789.34 cm^{-1}, and the C=O peak from 1689.64 cm^{-1} to 1631.77 cm^{-1}.These shifts indicate strong interactions between Ag_2O nanoparticles and the zirconium-based coordination polymer framework, likely due to metal–ligand coordination and changes in bond environment. Formation of the composite was proven by the peaks at 883.39 cm^{-1} and 1689.64 cm^{-1}shifting to 789.34 cm^{-1} and 1631.77 cm^{-1}, respectively. Similar IR spectral shifts have been observed in previous studies. Kayed et al. reported red shifts in Ag–O vibrations upon embedding Ag nanoparticles within Ag_2O, indicating altered electronic surroundings [34]. Likewise, Pasieczna-Büchner et al. showed that metal–organic interactions lead to shifts in functional group vibrations (such as C=O) due to coordination and electronic redistribution in the composite structure [35].

UV-Vis

The UV-Vis spectra of the synthesized products were recorded to examine their optical characteristics (such as optical absorption and band gap) and to confirm the formation of the composite.

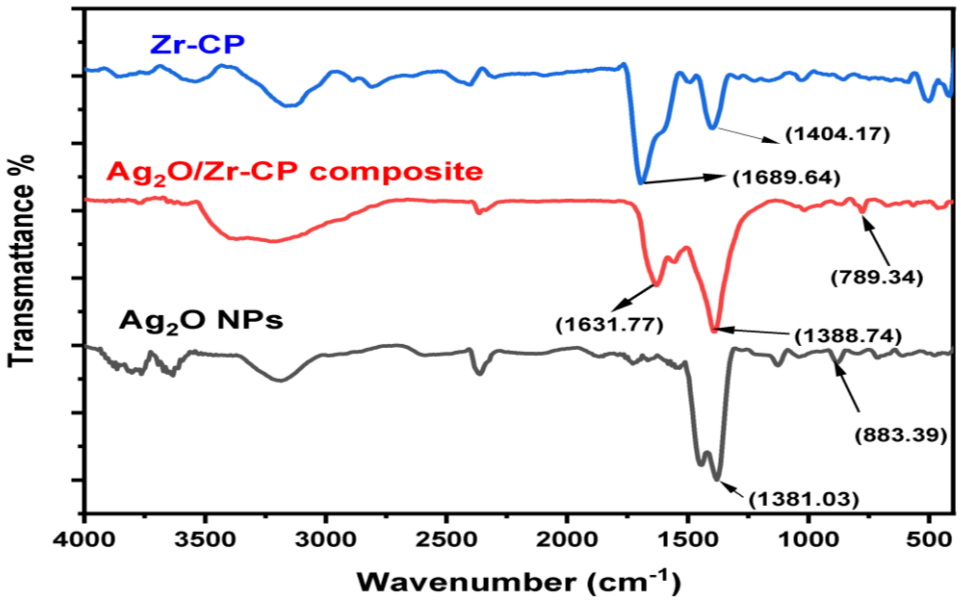

Figure 3. FTIR spectra of Zr-CP, Ag_2O/Zr-CP composite and Ag_2O NPs.

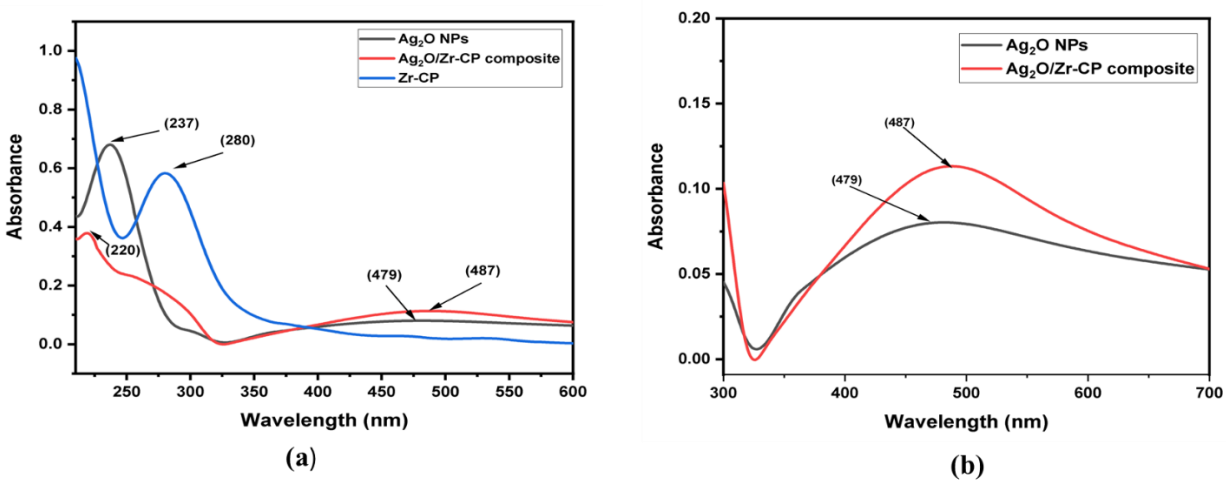

Figure 4. UV-Vis spectra of the Ag_2O NPs, Ag_2O /Zr-CP composite and Zr-CP.

Figure 4 demonstrates the UV–Vis absorption spectra of the Ag_2O NPs, Ag_2O/Zr-CP composite and Zr-CP. The UV-Vis spectrum of the Ag_2Onanoparticles exhibited a peak at 237 nm (due to charge transfer transitions) and a broad peak at 479 nm (ligand-to-metal charge transfer (LMCT),while that of Zr-CP had a peak at 280 nm due to π–π* transitions. For the Ag_2O/Zr-CP composite, optical absorptions took place at 220 nm and 487 nm. The π→π* transition of Zr-CP shifted to a lower wavelength (blue shift) in the composite (280 nm to 220 nm). This shift indicates electronic interactions between Zr-CP and the Ag_2O NPs. The slight redshift of the Ag_2O peak (479 nm to 487 nm) in the composite suggests strong interfacial interactions with Zr-CP. These shifts in wavelength provide clear evidence of Ag_2O/Zr-CP composite formation. Similar spectral shifts have been reported in previous studies. Shi et al. (2014) observed red shifts in the LMCT band of Ag_2O when incorporated into g-C_3N_4, which they attributed to interfacial charge transfer and strong coupling [36]. Likewise, Mishra and Chun explained that blue or red shifts in UV–Vis spectra can result from quantum confinement, metal–ligand interactions, or modification of the local electronic environment during composite formation [37].

Band Gap Analysis

The Ag_2O/Zr-CP composite had a bandgap of 1.8 eV, while the Ag_2O NPs had a bandgap of 1.62 eV, as shown in **Figure 5**. The bandgap of Zr-CP was approximately 2.2 eV [22].

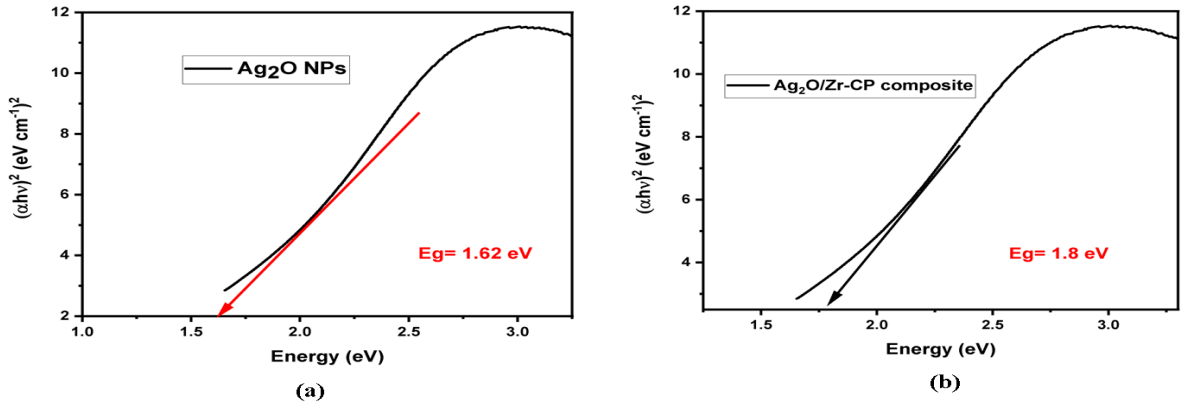

Figure 5. Tauc plots of band gap calculations for the (a) Ag_2O NPs and (b) Ag_2O/Zr-CP composite.

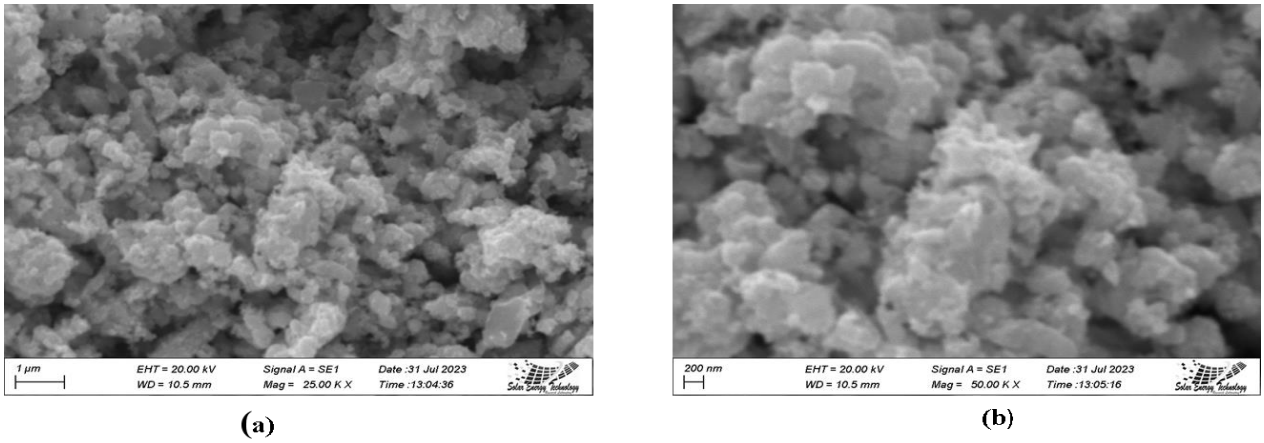

Figure 6. SEM images of (a) Ag_2O/Zr-CP composite at 25.00 KX and (b) Ag_2O/Zr-CP composite at 50.00 KX.

The reduction in the bandgap value of Zr-CP upon forming the Ag_2O/Zr-CP composite is likely due to the formation of a composite interface, where the electronic interaction between Ag_2O and Zr-CP facilitates band alignment and charge transfer. This interaction introduces new energy states between the conduction and valence bands, effectively narrowing the optical band gap and enhancing visible-light absorption. Such bandgap tuning is advantageous for photocatalysis, as it allows the composite to harness more of the solar spectrum. Similar bandgap narrowing due to Ag_2O incorporation has been reported in Ag_2O-based composites, such as Ag_2O/g-C_3N_4, where improved charge separation and red-shifted absorptions were observed [36]. The Tauc equation $\alpha=A(h\nu-E_g)\ n/h\nu$ was used for calculating bandgap values, where hv stands for photon energy, E_g for energy gap, A for proportionality constant, and α for absorption coefficient. This equation is commonly used to find a material's optical bandgap.

Scanning Electron Microscopy (SEM)

SEM is an important advanced technique that is used to produce intricate, high-resolution images by scanning the surface of a material. The images obtained from the SEM analysis provide comprehensive detailed information about the morphology and other surface properties of the samples. In this study, SEM analysis was performed to determine the morphology of the Ag_2O/Zr-CP composite and to assess its porosity.

Figure 6 visualises the surface details, where the porous and fluffy structure of the Ag_2O/Zr-CP composite can be observed. Each image has a length of 100 nm. Therefore, it can be concluded that the size of the Ag_2O/Zr-CP composite was in the nanometre range. The composite's morphology predominantly exhibited a porous and spongy structure. This suggests a high surface area, which is advantageous for photocatalytic applications. Similar features were reported by Shi et al. (2014) for Ag_2O/g-C_3N_4 composites, where the porous structure enhanced light absorption and surface reactivity [36]. Thus, the observed morphology supports the potential of the Ag_2O/Zr-CP composite for efficient environmental remediation.

EDS

EDS (Energy Dispersive X-ray Spectroscopy) is an analytical technique employed in conjunction with SEM and used to determine the elemental composition of materials. In this study, EDS was carried out to confirm the formation of the Ag_2O/Zr-CP composite. Different areas were examined, and the associated peaks are displayed in **Figure 7**. Both the Ag_2O NPs and Zr-CP can be observed in the EDS spectra of the synthesized composite.

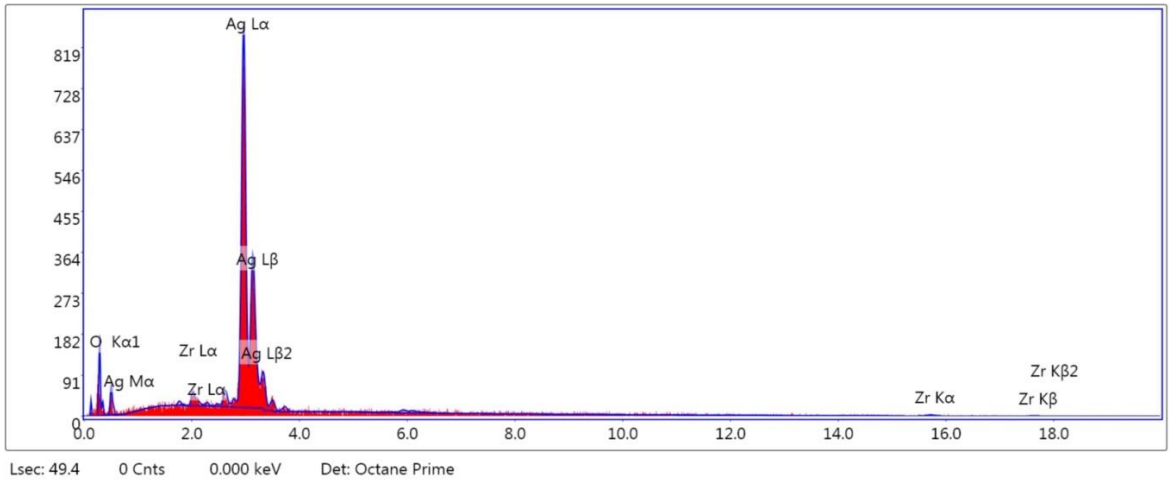

Figure 7.EDS spectra of the Ag_2O/Zr-CP composite.

Table 1.EDS weight ratios of the Ag_2O/Zr-CP composite.

Element	Weight (%)	Atomic (%)
Silver (Ag)	84.56	48.43
Oxygen(O)	12.91	49.86
Zirconium (Zr)	2.53	1.71

From the spectrum, the amounts of silver (Ag), oxygen (O) and zirconium (Zr) were determined to be 84.56, 12.91 and 2.53 weight %, respectively. **Table 1**provides detailed information of the composite's atomic and weight percentages from the EDS spectra. Zr-CP was a bulky, polymeric sponge-like compound and its void space was occupied by the Ag_2O NPs. Approximately 10 % of Zr was present in each monomer unit of Zr-CP.

A small amount (2.53 wt%) of Zr was observed in the Ag_2O/Zr-CP composite, as shown in **Table 1**. The low wt% of Zr observed may be attributed to the encapsulation of Ag_2O within the voids of the Zr-CP framework. Similar behaviour has been reported in MOF-based and g-C_3N_4 composites, where silver nanoparticles or silver oxide nanoparticles dominate the EDS spectra, while the lighter or embedded framework components appear in minor amounts. [36, 38].

Photocatalytic Activity

The evaluation of photocatalytic activity in the degradation of MB in wastewater is highly dependent on time. The UV–vis absorption spectra for the breakdown of MB under UV light exposure were recorded at 0, 15, 30, 45, and 60 minutes, respectively, with the Ag_2O NPs in **Figure 8(a)**, Ag_2O/Zr-CP composite in **Figure 8(b)** and TiO_2 in **Figure 8(c)**.

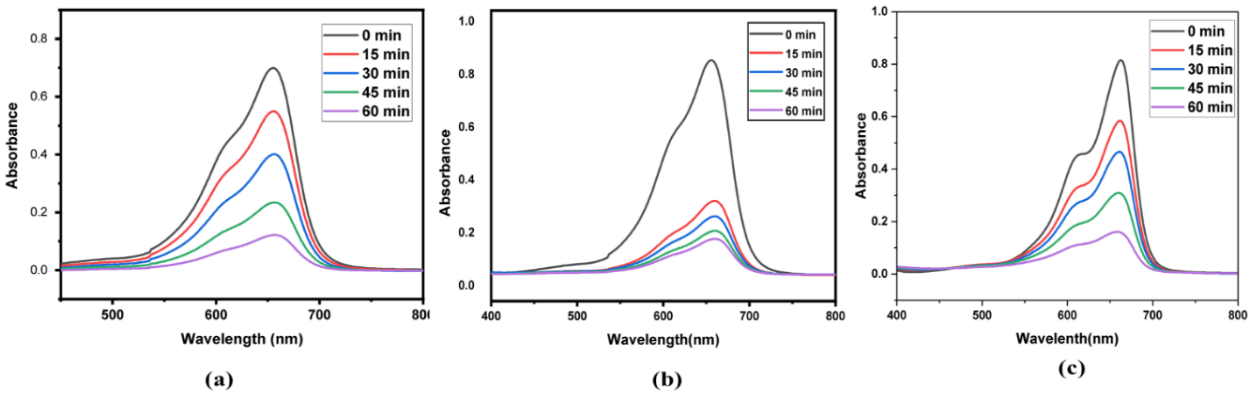

Figure 8. The degradation of MB by (a) Ag_2O NPs (b) Ag_2O/Zr-CP composite (c) TiO_2.

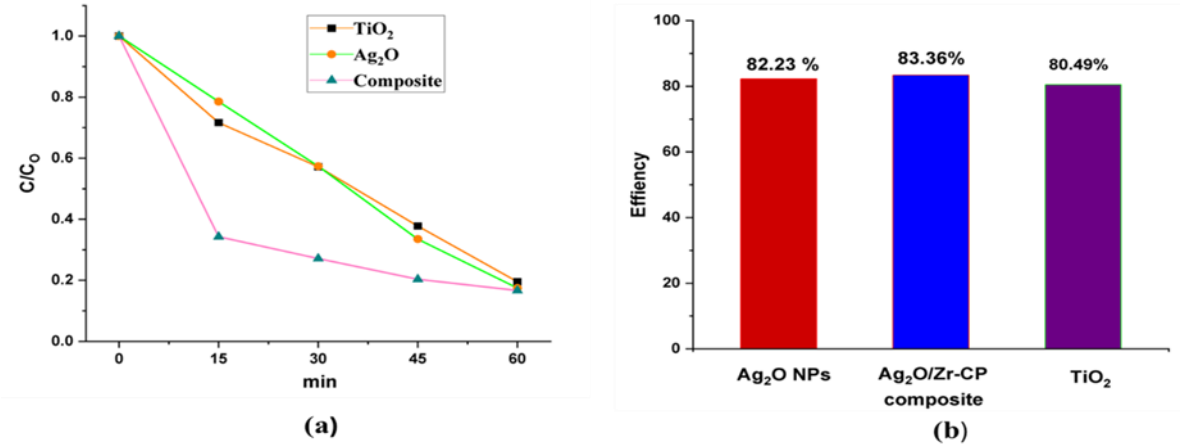

Figure 9. The decreasing trend in (a) C/C_o and (b) efficiency after 60 min of MB degradation by Ag_2O NPs, Ag_2O/Zr-CP composite and TiO_2.

According to the Beer-Lambert equation, absorption and concentration are directly proportional. As the irradiation time increased, the MB dye's absorption peak intensity gradually dropped in each case. This indicates that MB molecules were broken down by the Ag_2O NPs, Ag_2O/Zr-CP composites, and TiO_2.

The ratio of concentration at time 't' to the initial concentration (C_t/C_o) declined with time when the Ag_2O NPs, Ag_2O/Zr-CP composite, and TiO_2 were present as a photocatalyst, as depicted in **Figure 9(a).** After 60 minutes of irradiation, the degradation efficiencies of the Ag_2O NPs, Ag_2O/Zr-CP composite and TiO_2 were 82.23 %, 83.36 % and 80.49 %, respectively (**Figure 9(b)**). TiO_2 is an established photocatalyst [39]. The rate values obtained for the Ag_2O NPs and the Ag_2O/Zr-CP composite were 1.63×10^{-2} min^{-1} and 3.36×10^{-2} min^{-1}, respectively. The degradation efficiencies of both the Ag_2O NPs and the Ag_2O/Zr-CP composite were greater than that of TiO_2. Therefore, it can be concluded that the Ag_2O NPs and Ag_2O/Zr-CP composite were potent photocatalysts.

Photocatalytic Mechanism

Understanding the photocatalytic mechanism is essential to explain how the Ag_2O/Zr-CP composite degrades dye molecules under light irradiation. The following section outlines the fundamental process involved in photocatalysis, which supports the experimental results observed in this study. Photocatalysisis an oxidation process in which exposure to light causes complex compounds to break down into simpler, non-toxic fragments that have decreased molecular weights.

Photocatalyst, when radiated under suitable light and absorb it. The electron in the photocatalyst's valence band (VB) jumps into the conduction band (CB), leaving a hole in the VB. Both the electron and hole migrate to the surface of the photocatalyst. Electrons participate in reduction reactions and holes participate in oxidation reactions. These photoelectrons can be transferred to oxygen molecules that are present or be absorbed on the photocatalyst surface, or present in its proximity. These oxygen molecules accept electrons from the CB of the catalyst and are converted to superoxide anions ($\bullet O_2^-$). These anions are highly reactive and can participate in various redox reactions. They can further be used to degrade any kind of virus, bacteria or pollutant molecule into simpler molecules like CO_2 and H_2O. The holes produced can oxidize H_2O molecules that are absorbed over the catalyst or that are present in its proximity. These H_2O molecules are converted into hydroxyl radicals ($\bullet OH$) by donating electrons to holes present in the VB of the catalyst, thus converting it into a powerful oxidizing agent. Thus, these ions interact with organic pollutants or target molecules absorbed on the photocatalyst's surface, breaking them down into less harmful or inert substances. **Figure 10** shows the photocatalytic degradation mechanism of MB by Ag_2O NPs and the Ag_2O/Zr CP composite.

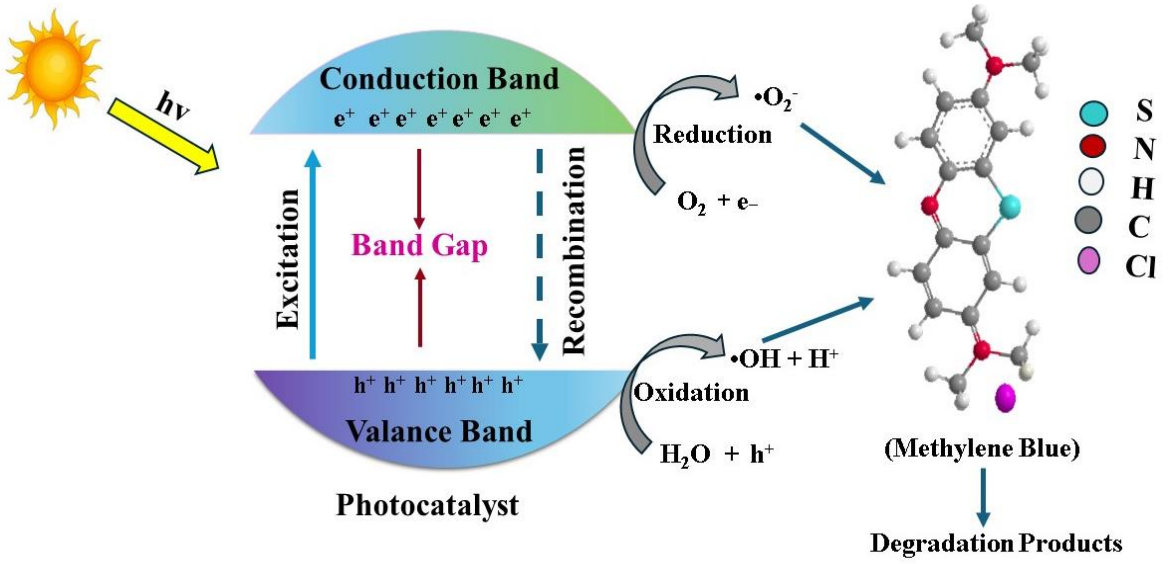

Figure 10. Photocatalytic degradation mechanism of methylene blue by Ag_2O NPs, and the Ag_2O/Zr-CP composite.

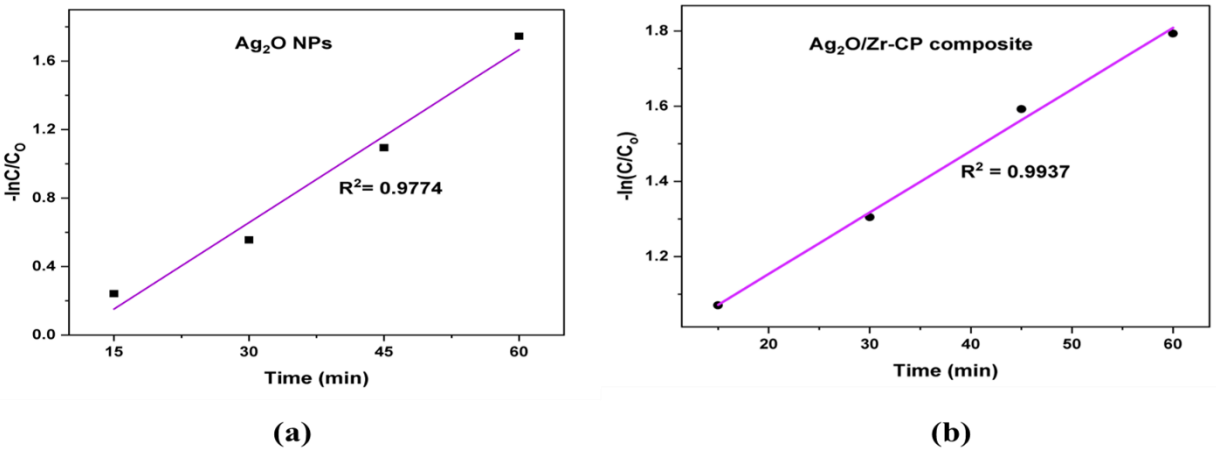

Figure 11. Pseudo-first order kinetics plots of MB adsorption the (a) Ag_2O NPs, and (b) Ag_2O/Zr-CP composite.

Kinetics of Photodegradation

To compare the photocatalysts and understand the reaction rates, the kinetics of the photodegradation of MB in the presence of the Ag_2O NPs and Ag_2O/Zr-CP composite were investigated as well. Plotting $-\ln(C/C_0)$ over time in **Figure 11(a, b)** determined the reaction rate constant and resulted in a straight line, where C_o is the absorbance at 0 min, and C is the absorbance at t min. The corresponding regression values (R^2) for the Ag_2O NPs and the Ag_2O/Zr-CP composite were found to be 0.9774 and 0.9937, respectively.

Thus, the degradation of MB dye using a photocatalyst followed first-order kinetics, with regression values for the fitted lines of $R^2 > 0.95$. [40]. The rate constant (k) of the photodegradation process was obtained from the slope of the plots. The obtained rate constant values of the Ag_2O NPs and Ag_2O/Zr-CP composite were 1.63×10^{-2} min^{-1} and 3.36×10^{-2} min^{-1}, respectively. This type of kinetic behaviour has been commonly observed in related photocatalytic studies and indicates the effectiveness of the photocatalyst in facilitating dye degradation via a first-order reaction mechanism [41].

CONCLUSION

A coprecipitation method and sonication technique were used to prepare the Ag_2O nanoparticles and Ag_2O/Zr-CP composite, respectively. FTIR and UV-

Vis spectroscopy confirmed that the Ag_2O NPs and Ag_2O/Zr-CP composite were formed. SEM analysis confirmed the nanostructures of the synthesized Ag_2O NPs and Ag_2O/Zr-CP composite. Ag_2O decreased the bandgap of Zr-CP in the Ag_2O/Zr-CP composite. The optimum bandgap values of the Ag_2O NPs and Ag_2O/Zr-CP composite facilitated the creation of electron-hole pairs in the photodegradation process. Under solar irradiation, the Ag_2O/Cu-CP composite showed significant photocatalytic activity in the breakdown of MB, compared to the Ag_2O NPs. Thus, the Ag_2O/Zr-CP composite may be used as a potent photocatalyst.

ACKNOWLEDGEMENT

The authors wish to thank Shahjalal University of Science and Technology, Research Center for the Promotional Research Grant (Project ID: PS/2024/1/02).

CONFLICT OF INTEREST

There is no conflict of interest to declare.

REFERENCES

1. Xu, G. R., An, Z. H., Xu, K., Liu, Q., Das, R. &Zhao, H. L. (2021) Metal organic framework (MOF)-based micro/nanoscaled materials for heavy metal ions removal: The cutting-edge study on designs, synthesis, and applications. *Coordination Chemistry Reviews*, **427**, 213554.

2. Sheta, S. M., Salem, S. R. & El-Sheikh, S. M. (2022) A novel Iron (III)-based MOF: Synthesis, characterization, biological, and antimicrobial activity study. *Journal of Materials Research*, **37(14)**, 2356–2367.

3. Motakef-Kazemi, N., Shojaosadati, S. A. & Morsali, A. (2014) In situ synthesis of a drug-loaded MOF at room temperature. *Microporous and mesoporous materials*, **186**, 73–79.

4. Noro, S. I., Kitagawa, S., Kondo, M. & Seki, K. (2000) A new, methane adsorbent, porous coordination polymer [{$CuSiF_6$(4,4′-bipyridine)$_2$}n]. *Angewandte Chemie International Edition*, **39(12)**, 2081–2084.

5. Min, K. S.& Suh, M. P. (2001) Self-assembly and selective guest binding of three-dimensional open-framework solids from a macrocyclic complex as a trifunctional metal building block. *Chemistry-A European Journal*, **7(1)**, 303–313.

6. Chen, D., Liang, F., Feng, D., Xian, M., Zhang, H., Liu, H. & Du, F. (2016) An efficient route from reproducible glucose to 5-hydroxymethylfurfural catalyzed by porous coordination polymer heterogeneous catalysts. *Chemical Engineering Journal*, **300**, 177–184.

7. Huang. Y. -B., Wang, Q., Liang, J., Wang, X., Cao, R. (2016) Soluble metal-nanoparticle-decorated porous coordination polymers for the homogenization of heterogeneous catalysis. *Journal of the American Chemical Society*, **138**, 10104–10107.

8. Zhou, Z., He, C., Yang, L., Wang, Y., Liu, T. & Duan, C. (2017) Alkyne activation by a porous silver coordination polymer for heterogeneous catalysis of carbon dioxide cycloaddition. *ACS Catalysis*, **7(3)**, 2248–2256.

9. d'Aquino, A. I., Kean, Z. S. & Mirkin, C. A. (2017) Infinite coordination polymer particles composed of stimuli-responsive coordination complex subunits. *Chemistry of Materials*, **29(24)**.

10. Zheng, Y. Z., Zheng, Z. & Chen, X. M. (2014) A symbol approach for classification of molecule-based magnetic materials exemplified by coordination polymers of metal carboxylates. *Coordination Chemistry Reviews*, **258**, 1–15.

11. Horcajada, P., Chalati, T., Serre, C., Gillet, B., Sebrie, C., Baati, T. & Gref, R. (2010) Porous metal–organic-framework nanoscale carriers as a potential platform for drug delivery and imaging. *Naturematerials*, **9(2)**, 172–178.

12. Chen, B., Wang, L., Zapata, F., Qian, G. & Lobkovsky, E. B. (2008) A luminescent microporous metal− organic framework for the recognition and sensing of anions. *Journal of the American Chemical Society*, **130(21)**, 6718–6719.

13. Fletcher, A. J., Thomas, K. M. & Rosseinsky, M. J. (2005) Flexibility in metal-organic framework materials: Impact on sorption properties. *Journal of Solid State Chemistry*, **178(8)**, 2491–2510.

14. Yao, H., Zhang, F., Zhang, G., Luo, H., Liu, L., Shen, M. & Yang, Y. (2018) A novel two-dimensional coordination polymer-polypyrrole hybrid material as a high-performance electrode for flexible super-capacitor. *Chemical Engineering Journal*, **334**, 2547–2557.

15. Cui, Y., Yue, Y., Qian, G. and Chen, B .(2012) Luminescent Functional Metal–Organic Frameworks. *Chemical Reviews*, **112**, 1126–1162.

16. Fujita, M., Umemoto, K., Yoshizawa, M., Fujita, N., Kusukawa, T. & Biradha, K. (2001) Molecular panelling via coordination. *Chemical Communications*, **6**, 509–518.

17. Somnath, Waris, Ali, A., Ahmad, M. & Siddiqui, K. A. (2022) Bifunctional self-penetrating Co(II)-Based 3D MOF for high-performance environmental and energy storage applications. *Crystal Growth & Design*, **22(12)**, 7374–7394.

18. Fakhri, H. & Bagheri, H. (2020) Highly efficient Zr-MOF@ WO_3/graphene oxide photocatalyst: Synthesis, characterization and photodegradation of tetracycline and malathion. *Materials Science in Semiconductor Processing*, **107**, 104815.

19. Ma, Z., Song, X., Li, Z., Ren, Y., Wang, J. & Liang, Y. (2024) Ag-based coordination polymer-enhanced photocatalytic degradation of ciprofloxacin and nitrophenol. *Dalton Transactions*, **53(8)**, 3797–3807.

20. Suppaso, C., Kamakura, Y., Ueno, M., Hongo, S., Akiyoshi, R., Ishiwari, F. & Maeda, K. (2024) Facile Room Temperature Synthesis of Precious-Metal-Free Coordination Polymer Photocatalyst for Improved Visible-Light CO_2 Reduction. *Solar RRL*, **8(1)**, 2300710.

21. Furukawa, H., Cordova, K. E., O'Keeffe, M. and Yaghi, O. M. (2013) The Chemistry and Applications of Metal–Organic Frameworks. *Science*, **341**, 1230444.

22. Alam, M. M., Ahmed, M. F., Arafath, M. A., Karim, M. R., Uddin, M. N. & Hossain, M. S.(2024) Synthesis of Cu and Zr-based coordination polymers with N/O donors and investigation of their photocatalytic activity against dye. *Heliyon*, **10(12)**, e33440.

23. Karunakaran, S. T., Pavithran, R., Sajeev, M. &Rema, S.M. M. (2022) Photocatalytic degradation of methylene blue using a manganese-based metal organic framework. *Results in Chemistry*, **4**, 100504.

24. Chen, Y., Zhai, B., Liang, Y., Li, Y. & Li, J.(2019) Preparation of CdS/g-C_3N_4/MOF composite with enhanced visible-light photocatalytic activity for dye degradation. *Journal of SolidState Chemistry*, **274**, 32–39.

25. Baig, N., Kammakakam, I. &Falath, W. (2021) Nanomaterials: A review of synthesis methods, properties, recent progress, and challenges. *Materials Sdvances*, **2(6)**, 1821–1871.

26. Jamkhande, P. G., Ghule, N. W., Bamer, A. H. & Kalaskar, M. G. (2019) Metal nanoparticles synthesis: An overview on methods of preparation, advantages and disadvantages, and applications. *Journal of Drug Delivery Science and Technology*, **53**, 101174.

27. Moura, D., Souza, M. T., Liverani, L., Rella, G., Luz, G. M., Mano, J. F. & Boccaccini, A. R. (2017). Development of a bioactive glass-polymer composite for wound healing applications. *Materials Science and Engineering: C*,**76**, 224–232.

28. Gawande, M. B., Goswami, A., Felpin, F. X., Asefa, T., Huang, X., Silva, R. & Varma, R. S. (2016) Cu and Cu-based nanoparticles: synthesis and applications in catalysis. *Chemical Reviews*, **116(6)**, 3722–3811.

29. Zhang, D., Cui, S. & Yang, J. (2017) Preparation of Ag_2O/g-C_3N_4/Fe_3O_4 composites and the application in the photocatalytic degradation of Rhodamine B under visible light. *Journal of Alloys and Compounds*, **708**, 1141–1149.

30. Ullah, R., Tuzen, M. & Hazer, B. (2023) Novel silver-morphine-functionalized polypropylene (AgPP-mrp) nanocomposite for the degradation of dye removal by multivariate optimization approach. *Environmental Science and Pollution Research*, **30(33)**, 79904–79915.

31. Hosseinpour, S. A., Karimipour, G., Ghaedi, M. &Dashtian, K. (2018) Use of metal composite MOF-5-Ag_2O-NPs as an adsorbent for the removal of Auramine O dye under ultrasound energy conditions. *Applied Organometallic Chemistry*, **32(2)**, e4007.

32. Balu, S., Uma, K., Pan, G. T., Yang, T. C. K. & Ramaraj, S. K. (2018) Degradation of methylene blue dye in the presence of visible light using SiO_2@ α-Fe_2O_3 nanocomposites deposited on SnS_2 flowers. *Materials*, **11(6)**, 1030.

33. Asif, M., Iqbal, W., Fakhar-e-Alam, M., Hussain, Z., Saadullah, M., Hassan, M. & Al-Qahtani, N. H. (2024) Synthesis and Characterization of Chemically and Green-Synthesized Silver Oxide Particles for Evaluation of Antiviral and Anti-cancer Activity. *Pharmaceuticals*,**17(7)**, 908.

34. Kayed, K., Issa, M. & Al-Ourabi, H. (2024) The FTIR spectra of Ag/Ag_2O composites doped with

silver nanoparticles. *Journal of Experimental Nanoscience*, **19(1)**, 2336227.

35. Pasieczna-Patkowska, S., Cichy, M. & Flieger, J. (2025) Application of Fourier transform infrared (FTIR) spectroscopy in characterization of green synthesized nanoparticles. *Molecules*, **30(3)**, 684.

36. Shi, L., Liang, L., Ma, J., Wang, F. & Sun, J. (2014) Enhanced photocatalytic activity over the Ag_2O–gC_3N_4 composite under visible light. *Catalysis Science & Technology*, **4(3)**, 758–765.

37. Mishra, M. & Chun, D. M. (2015) α-Fe_2O_3 as a photocatalytic material: A review. *Applied Catalysis A: General*, **498**, 126–141.

38. Surya, S. G., Bhanoth, S., Majhi, S. M., More, Y. D., Teja, V. M. & Chappanda, K. N. (2019) A silver nanoparticle-anchored UiO-66 (Zr) metal–organic framework (MOF)-based capacitiveH_2S gas sensor. *Cryst. Eng. Comm.*, **21(47)**, 7303–7312.

39. Chen, D., Cheng, Y., Zhou, N., Chen, P., Wang, Y., Li, K. & Ruan, R. (2020) Photocatalytic degradation of organic pollutants using TiO_2-based photocatalysts: A review. *Journal of Cleaner Production*, **268**, 121725.

40. Alkaykh, S., Mbarek, A. & Ali-Shattle, E. E. (2020) Photocatalytic degradation of methylene blue dye in aqueous solution by $MnTiO_3$ nanoparticles under sunlight irradiation. *Heliyon*, **6(4)**.

41. Chen, B., Wang, L., Zapata, F., Qian, G. & Lobkovsky, E. B. (2008) A luminescent microporous metal− organic framework for the recognition and sensing of anions. *Journal of the American Chemical Society*, **130(21)**, 6718–6719.